UNIVERSITY *of* York

This is a repository copy of *Direct observation of spin polarization in epitaxial Fe3O4(001)/MgO thin films grown by magnetron sputtering*.

Direct observation of spin polarization in epitaxial Fe₃O₄(001)/MgO thin films grown by magnetron sputtering

Zhe Zhang,[1, #] Xianyang Lu, [1, 2, #, a)] Yu Yan,[1, 2] Jiahua Lu,[1] Zhuoyi Li,[1] Qi Liu,[1] Fangyuan Zhu,[3] Jiefeng Cao,[3] Yong Wang,[3] Zhaocong Huang,[4] Ya Zhai,[4] Yao Li,[1] Xuezhong Ruan,[1] Liang He,[1] Jing Wu[2], Jun Du,[5] Rong Zhang[1], Yongbing Xu[1, 2, a)]

[1]Jiangsu Provincial Key Laboratory of Advanced Photonic and Electronic Materials, School of Electronic Science and Engineering, Nanjing University, Nanjing 210093, China
[2]York-Nanjing International Joint Center in Spintronics, Department of Electronics and Physics, University of York, York YO10 5DD, of *UK*
[3]Shanghai Synchrotron Radiation Facility, Shanghai Advanced Research Institute, Chinese Academy of Sciences, Shanghai 201204, China
[4]Department of Physics, Southeast University, Nanjing 211189, China
[5]Department of Physics, Nanjing University, Nanjing 210093, China

We obtained epitaxial single-crystal Fe₃O₄(001)/MgO(001) thin films by magnetron sputtering. The high quality of the grown Fe₃O₄ films was confirmed by reflection high-energy electron diffraction (RHEED) and X-ray photoelectron spectroscopy (XPS). The atomic magnetic properties of Fe₃O₄(001)/MgO(001) were investigated using vibrating sample magnetometry (VSM) and X-ray magnetic circular dichroism (XMCD). The values of saturation magnetization and magnetic moment are 407 ± 5 emu/cm³ (3.26 ± 0.04 $\mu_B/(f.u.)$) and 3.31 ± 0.15 $\mu_B/(f.u.)$ in the Fe₃O₄ film as thin as 5 nm, which are close to the bulk values. The spin polarization was directly measured using spin-resolved photoemission spectroscopy (SRPES). The measured spin polarization has a maximum value of -$42\pm3\%$, which is comparable to the theoretical value for the $(\sqrt{2}\times\sqrt{2})R45°$ reconstructed Fe₃O₄(001) surface. Furthermore, the film thickness-dependent measurements indicate that the anti-phase boundaries (APBs) significantly decrease the spin polarization rather than the lattice mismatch. Our results demonstrate that the epitaxial Fe₃O₄(001)/MgO thin films grown by magnetron sputtering have desired magnetic properties, facilitating the potential application of Fe₃O₄-based spintronic devices.

a)Authors to whom correspondence should be addressed: xylu@nju.edu.cn and ybxu@nju.edu.cn
#Z. Zhang and X. Lu contributed equally to this work

1

In the past few decades, great progress has been made in the research field of spintronic devices. In these devices, effective injection and detection of spin-polarized currents via ferromagnetic (FM) materials are the key. Half-metallic ferromagnets (HMFs), owing to their predicted 100% spin polarization at the Fermi level, have attracted great attention since it was first proposed in the early 1980s[1]. Among HMF materials, magnetite (Fe_3O_4) has attracted more attention due to its stability at high temperatures. Moreover, Fe_3O_4 exhibits robust ferrimagnetism with a Curie temperature T_C=851 K. A 100% spin polarization near the Fermi level (E_F) is theoretically predicted in Fe_3O_4 with a conductive minority spin channel and a semiconducting majority spin channel[2,3]. This makes Fe_3O_4 attract more interest as a potential material for next-generation spintronic devices[4-6].

Fe_3O_4 films can be prepared by three methods: pulsed laser deposition (PLD)[7], molecular beam epitaxy (MBE)[8], and magnetron sputtering. Compared with the other two methods, the magnetron sputtering method is easy to implement, simple and efficient. The films grown by magnetron sputtering are generally more compact and uniform. Therefore, it is more convenient to use in device fabrication and industrial production. Yanagihara *et al*. grew spinel-type epitaxial Fe_3O_4(001) films using reactive sputtering by introducing O_2 gas into an Ar base gas during film growth in a radio frequency (RF) planar magnetron sputtering apparatus[9]. However, studies on spin polarization and atomic magnetization in Fe_3O_4 films prepared by magnetron sputtering are limited.

In this work, high-quality epitaxial $Fe_3O_4(001)$ thin films grown on MgO(001) substrates using RF magnetron sputtering were confirmed by a series of characterization experiments. The values of the magnetization and the atomic moment are found to be close to the bulk values when the film thickness is larger than 5 nm. A maximum value of spin polarization of $-42\pm3\%$ is observed for 40 nm $Fe_3O_4(001)$ films, which is close to the theoretically predicted value. Importantly, the thickness-dependent measurements demonstrate that the spin polarization of the nanoscale $Fe_3O_4(001)$/MgO films is significantly affected by the anti-phase boundary defects rather than the lattice mismatch.

High-quality Fe_3O_4 (001) films were grown on single-crystal MgO(001) substrates by introducing O_2 gas into an Ar base gas during film growth in our magnetron sputtering system with a base pressure of 1×10^{-8} Torr. The MgO(001) substrates were annealed at 500 °C for 60 min until a smooth surface could be identified via the sharp reflection high-energy electron diffraction (RHEED) patterns, as shown in Fig. 1(a). During the film growth process, a 50 sccm Ar (99.999%) gas flow was introduced, while the flow rate of O_2 (99.999%) was controlled from 0.0 to 2.0 sccm. The total gas pressure was maintained at about 4×10^{-3} Torr. A pure iron target (99.95%) was used, and the RF power was set as 50 W. The substrate temperature was fixed at 300 °C during the deposition process. After deposition, RHEED measurements were *in-situ* performed. By measuring the spacing of the streaks in RHEED images using KSA 400 software, we can determine the lattice constant of films with different lattice structures. The structural and elemental analysis of the grown films were *ex-situ* carried out by X-ray

3

diffraction (XRD), X-ray photoelectron spectroscopy (XPS) and Raman spectroscopy.

The grown films were immediately transferred from the growth chamber to the spin-resolved photoemission spectroscopy (SRPES) chamber via a UHV (5×10^{-10} Torr) interconnected tube. Thus, the SRPES measurements can be *in-situ* performed on a high-quality sample surface. The base pressure of the analyzer chamber is under 2×10^{-10} mbar, and the energy resolution is 35 meV at room temperature. A helium lamp is applied to generate ultraviolet light with a photon energy of 21.218 eV (He-I). All SRPES measurements were performed at room temperature.

The static magnetic hysteresis loops along the MgO[0-11] direction are measured by a vibrating sample magnetometer (VSM) at room temperature. X-ray magnetic circularly dichroism (XMCD) measurements at the Fe $L_{2,3}$ absorption edges were performed at beamline BL07U of the Shanghai Synchrotron Radiation Facility. The X-ray absorption (XAS) was measured at room temperature under an applied magnetic field of 3 T along the out-of-plane direction by total electron yield (TEY) detection. The 100% circularly polarized X-rays were used in normal incidence with respect to the sample plane and in parallel with the applied magnetic field. By flipping the X-ray helicity at a fixed magnetic field, we can obtain the XMCD of our samples.

It is well known that both the rock salt structure of MgO and the inverse spinel structure of Fe_3O_4 are based on a fcc oxygen anion lattice. This allows a continuous oxygen sublattice over the MgO/Fe_3O_4 interface[10]. The lattice constant of Fe_3O_4 8.396 Å is approximately twice that of MgO 4.216 Å, resulting in a very small lattice mismatch. As shown in Fig. 1(b), a clear and sharp RHEED pattern indicates that the

4

Fe film deposited with a 0 sccm O_2 flow rate has a bcc structure with an epitaxial relationship of Fe(001)[0-11]//MgO(001)[001]. Fig. 1(c) shows the RHEED pattern of the 20 nm Fe_3O_4 film grown on a MgO(001) substrate at an O_2 flow rate of 1.5 sccm with an epitaxial relationship of Fe_3O_4(001)[001]//MgO(001)[001]. The image confirms a specific $\left(\sqrt{2} \times \sqrt{2}\right)R45°$ reconstruction of the Fe_3O_4(001) surface[11]. Clear and sharp lines with a Laue ring also confirm that our grown film exhibits good crystallinity with a flat well-ordered surface. When the O_2 flow rate increased to 2 sccm, we obtained a γ-Fe_2O_3 film, as shown in Fig. 1(d). It is worth mentioning that the ε-Fe_2O_3 phase will not occur unless the growth temperature increases to 800 °C[12].
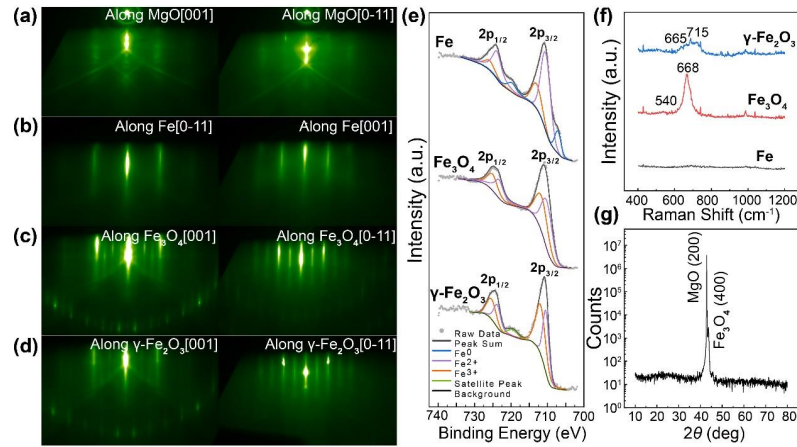

FIG 1. RHEED patterns of the (a) MgO(001) substrate. (b) 20 nm Fe film grown at 0 sccm flow rate of O_2. (c) 20 nm Fe_3O_4 film grown at 1.5 sccm flow rate of O_2. (d) 20 nm γ-Fe_2O_3 film grown at a 2 sccm flow rate of O_2. (e) Fe 2p XPS spectra of 20 nm Fe, Fe_3O_4, and γ-Fe_2O_3 films. (f) Raman spectra of 20 nm Fe, Fe_3O_4, and γ-Fe_2O_3 films. (g) XRD spectrum of 50 nm Fe_3O_4 film.

The Fe 2p core-level XPS spectra of the films deposited at different O_2 flow rates

are presented in Fig. 1(e). The XPS spectra were fitted by using XPS peak 4.1 software. As shown in the middle row, the spectrum of a 20 nm Fe_3O_4 film deposited at 1.5 sccm of O_2 shows two Fe_3O_4 characteristic peaks at 711 and 724 eV, corresponding to the binding energies of Fe^{2+} $2p_{3/2}$ and Fe^{2+} $2p_{1/2}$[13,14]. The films were also analyzed by Raman spectroscopy, as shown in Fig. 2(f). We can observe one major component situated at 668 cm^{-1} and a minor component at approximately 540 cm^{-1} for Fe_3O_4. The major Raman peaks for γ-Fe_2O_3 appear at 665 cm^{-1} and 715 cm^{-1}, which are in good agreement with the results obtained in other studies[15,16]. We also carried out XRD measurements of a 50 nm Fe_3O_4 film. As shown in Fig. 1(g), the observation of clear and sharp MgO (200) and Fe_3O_4 (400) peaks confirms that our Fe_3O_4 films have a good (001) orientation. Through the above analysis, we can observe a clear oxidation process, and the best flow rate of O_2 for Fe_3O_4 growth is 1.5 sccm.

The magnetic hysteresis loops as a function of the Fe_3O_4 film thickness with an applied magnetic field along the MgO[0-11] direction are shown in Fig. 2(b). The M_S increases with the thickness and reaches a maximum of 407±5 emu/cm^3 (3.26±0.04 $\mu_B/(f.u.)$) at 5 nm, which is lower than the value of 480 emu/cm^3 for bulk magnetite. The Fe $L_{2,3}$-edge XAS and XMCD spectra of films deposited at 0, 1.5, and 2 sccm O_2 are shown in Fig. 2(a). For Fe_3O_4, due to the antiparallel spin orientations of the A and B sites, the characteristic contributions from different sites of Fe_{td}^{3+}, Fe_{oh}^{2+}, and Fe_{oh}^{3+} in Fe_3O_4 can be identified. For γ-Fe_2O_3, the XMCD signal was derived from the superposition of the contributions of Fe^{3+} ions at both the A and B sites[17]. All of the measured XMCD spectra are in agreement with reported studies[17-19]. The values of spin

6

moment m_s and orbital moment m_l were calculated by applying sum rules on the integrated XMCD and total XAS spectra of Fe $L_{2,3}$ edges based on Eq. (1),

$$m_l = -\frac{4}{3}n_h \frac{\int_{L_{2,3}}(\sigma^+ - \sigma^-)dE}{\int_{L_{2,3}}(\sigma^+ + \sigma^-)\,dE}$$

$$m_s + \langle T_z \rangle = -n_h \frac{6\int_{L_3}(\sigma^+ - \sigma^-)dE - 4\int_{L_{2,3}}(\sigma^+ - \sigma^-)\,dE}{\int_{L_{2,3}}(\sigma^+ + \sigma^-)\,dE}, \qquad (1)$$

where $n_h = 6.61$ is the effective number of 3d-band holes[19]. The magnetic dipole term $\langle T_z \rangle$ is negligible because of the predominantly cubic symmetry of magnetite. The background of each XAS spectrum was fitted by an arctangent-based step function[20], as shown in Fig. 2(a). From the 5 nm Fe_3O_4 film deposited at an O_2 flow rate of 1.5 sccm, we obtained the values of $m_s = 2.64 \pm 0.1$ μ_B/f. u. and $m_l = 0.67 \pm 0.05$ μ_B/f. u., while the total moment $m_{l+s} = 3.31 \pm 0.15$ μ_B/f. u. and the orbital to spin moment ratio $m_l/m_s = 0.25$. The epitaxial Fe_3O_4/MgO(001) thin film exhibits a considerably large m_l, but its m_{l+s} is less than the bulk value (4.0 $\mu_B/(f. u.)$). Table SI gives an overview of the spin and orbital moment of the magnetite. Among these results, Babu et al. observed a sizeable $m_l = 0.44 \pm 0.05$ μ_B/f. u. in Fe_3O_4/BaTiO$_3$[21], while an unquenched m_l of 0.47 ± 0.05 μ_B/f. u. was also observed by Liu et al. in Fe_3O_4/MgO/GaAs[18]. Our results are in good agreement with these works, and the observation of a large m_l is of significance for spintronics applications as high <LS> coupling is essential for the ultrafast switching of spin polarization by electric field and circularly polarized light[22-25].

Fig. 2(c) shows the saturation magnetization (M$_S$) and atomic magnetic moment of Fe_3O_4 films deposited at 1.5 sccm with different film thicknesses. The M$_S$ and

7

Applied Physics Letters

magnetic moment increase as a function of film thickness and reach maximum values at a thickness of 5 nm. This observation is consistent with the lattice constant data shown in Fig. 4. It is indicated that when the thickness is less than 5 nm, the lattice mismatch between the grown layer and the substrate is larger, resulting in a corresponding decrease in the M_S and magnetic moment. Another reason for the low M_S and magnetic moment in thin films may be the interdiffusion between Mg^{2+} and Fe ions at the interface[26]. Our films are grown at 300°C, so this diffusion is to be expected. The maximum values of M_S and the magnetic moment we observed are reduced compared with the bulk values, which may be due to the formation of antiphase boundaries (APBs) in Fe_3O_4. Such antiferromagnetic exchange interactions between the boundaries usually lead to a saturation field as large as 7 T[18,27,28]. Our applied magnetic field of 3 T is not large enough to rule out the effects of APBs during our measurements. The values of M_S are in line with the value of the magnetic moment after converting emu/cm^3 to $\mu_B/f.u.$ when the thickness reaches 5 nm. However, the minimum value of the magnetic moment at 1 nm (1.80 ± 0.05 $\mu_B/f.u.$) is smaller than the value of M_S (2.82 ± 0.04 $\mu_B/f.u.$). This provides further evidence that APBs play a significant role in the measurements of XMCD when the Fe_3O_4 thickness is relatively small. Nevertheless, it is clearly shown that the values of magnetization and the atomic moment change obviously with film thickness. When the thickness of our grown Fe_3O_4 reaches 5 nm, the values of M_s and the total magnetic moment are close to the bulk value.
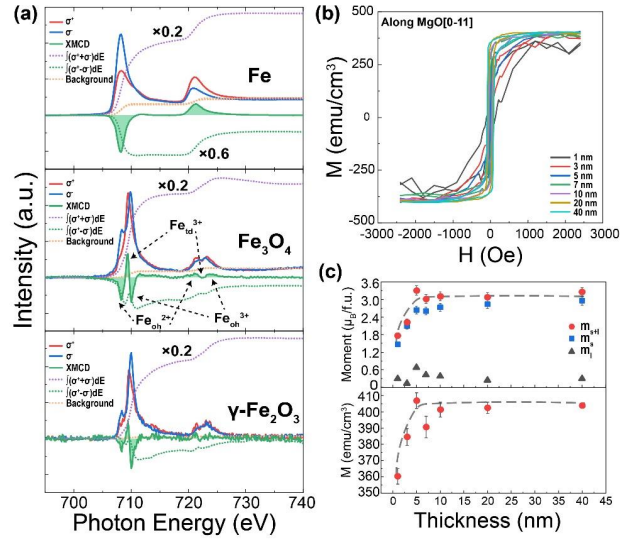
FIG 2. (a) Fe $L_{2,3}$-edge XAS and XMCD spectra of 20 nm Fe (0 sccm O_2), 5 nm Fe_3O_4 (1.5 sccm O_2) and 20 nm γ-Fe_2O_3 (2 sccm O_2). (b) VSM magnetization curves of Fe_3O_4 films with different thicknesses. (c) M_S and moment of Fe_3O_4 films with different thicknesses. The dashed lines are guidelines for the eye.

SRPES measurements were *in-situ* performed, and the spin polarization P is defined as $P = \frac{1}{S_{eff}} \frac{I_+ - I_-}{I_+ + I_-}$, where the effective Sherman function $S_{eff} = 0.16 \pm 0.01$ is used and I_+ and I_- are the spectra acquired by the two channeltrons in opposite spin directions. The SRPES spectra and the corresponding spin polarization of Fe_3O_4 films with different thicknesses are shown in Fig. 3. The spin polarization changed dramatically with the Fe_3O_4 thickness. When the thickness increased to 5 nm, we can observe a typical spin polarization curve of Fe_3O_4. The 40 nm Fe_3O_4 film deposited at 1.5 sccm has a spin polarization value up to -42±3% near the Fermi level. The absolute value of the spin polarization decreases and switches sign at 1.0 eV. It exhibits a maximum value with further increasing binding energies and becomes negative again

9

at 1.8 eV. Our results are in good agreement with the theoretically predicted values of spin polarization at the Fermi level, considering surface reconstruction and stabilization[29]. The surfaces of magnetite tend to reconstruct due to their polar nature, and thus their magnetic and electronic properties may strongly deviate from each other and from the bulk. The intrinsic instability of the magnetite (100) and (111) surfaces is known to result in a variety of possible metastable reconstructions[30]. For Fe_3O_4 (001), a larger $(\sqrt{2} \times \sqrt{2})R45°$ reconstruction was observed experimentally[11,31] instead of the (1×1) bulk-like termination. The atomic structure of this reconstruction surface is terminated by octahedrally coordinated iron atoms arranged in rows, referred to as a *modified B layer*[29,32]. From the RHEED patterns shown in Fig. 1(c), we observed a specific $(\sqrt{2} \times \sqrt{2})R45°$ reconstruction of the $Fe_3O_4(001)$ surface, similar to other reports[11]. The reconstruction and stabilization of the (001) surface lead to lattice distortions and consequently change the electronic properties. The DFT results reported by M. Foini et al. on the $Fe_3O_4(001)$ surface show a smaller value of -40% of the spin polarization at the Fermi level (E_F) compared to the bulk density of state[29], which agrees very well with our results. The spin polarization close to E_F reported by W. Wang *et al*. reaches -50% and -72% for 6.20 and 4.65 eV photons, respectively[33]. The high value of spin polarization they observed can be explained by an increase of the inelastic mean-free path. When a light source with lower photon energy is used, the inelastic mean-free path of electrons will increase, which could lead to a more efficient probe of bulk properties. The effect of self-energy renormalization on the majority spin states near E_F, resulting in an increase in spectral functions, can also reduce the spin polarization[34].
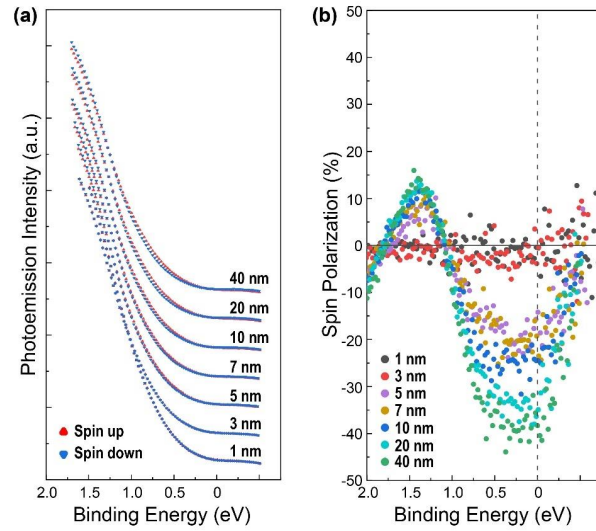
10

FIG 3. (a) Spin-resolved photoemission spectra of Fe_3O_4 (1.5 sccm O_2) with different thicknesses. (b) Spin polarization of Fe_3O_4 with different thicknesses.

The spin polarization of $Fe_3O_4(001)$ films with respect to the film thickness is investigated. As shown in Fig. 4(a), the spin polarization increases with increasing thickness. Specifically, the spin polarization is almost zero at 1 nm. When the Fe_3O_4 thickness increases to 5 nm, the spin polarization increases significantly to -22±3%. Correspondingly, the lattice constant significantly changes at a thickness of 5 nm, as shown in the inset of Fig. 4(a), which means a decrease in lattice distortion. This result suggests a strong effect on the electronic properties caused by lattice distortions, which reduce the spin polarization in ultrathin Fe_3O_4 (001) films. Then, the value of spin polarization increases to -38±5% at a thickness of 20 nm and reaches -42±3% at a

11

thickness of 40 nm. However, when the thickness is larger than 5 nm, the lattice constant

is almost unchanged and close to the bulk value of Fe_3O_4. This suggests that lattice

distortion is not the reason for the spin polarization change when the film thickness is

larger than 5 nm. As reported by Liu et al., the measured magnetoresistance decreases

from −6.5% to −1.1% as the thickness of Fe_3O_4 decreases from 80 to 5 nm, which is

explained by the enhanced spin-flip scattering at film and grain surfaces[35]. This

enhanced spin-flip scattering could also account for the reduced spin polarization in

thinner films. Another factor is the antiphase boundaries (APBs), which are common in

magnetite films[36-38]. The SRPES measurements were performed in the remanent (M_r)

state after being magnetized along the in-plane MgO[0-11] direction. The exchange

coupling between the APBs defects is antiferromagnetic, therefore a higher M_r reflects

a lower density of APBs. The film thickness dependence of M_r, shown in Fig. 4(b), is

in good agreement with the observed spin polarization. The remanence, as well as the

spin polarization, reach its maximum values at about 20 nm. Therefore, the APBs play

a significant role in the measurements of spin polarization, especially when the film

thickness is less than a critical value of 20 nm. Nevertheless, the spin polarization of

the Fe_3O_4 film close to the theoretical value is observed in the film as thin as 20 nm.

When the film thickness is larger than the critical thickness, the magnetron sputtering

grown Fe_3O_4 films have ideal magnetic properties close to the bulk values, including

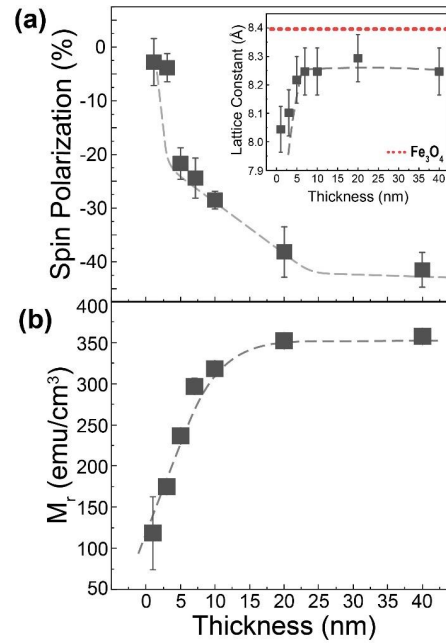the magnetic hysteresis loops and the spin polarization near the Fermi level.

FIG 4. (a) Spin polarization near the Fermi level of Fe_3O_4 (1.5 sccm O_2) films with different thicknesses. Illustration: Lattice constant of Fe_3O_4 films with different thicknesses. (b) Remanence (M_r) of Fe_3O_4 films with different thicknesses. The dashed lines are guidelines for the eye.

To summarize, we have demonstrated the epitaxial growth of single-crystal $Fe_3O_4(001)$ ultrathin films on $MgO(001)$ substrates by sputtering an iron target in an Ar-O_2 mixed gas. The flow rate near 1.5 sccm of O_2 is the optimal condition for growing Fe_3O_4 films. The formation of high-quality ferrimagnetic Fe_3O_4 was confirmed by RHEED and XPS. The VSM and XMCD results show that when the thickness of the Fe_3O_4 film reaches 5 nm, the value of M_s and the total magnetic moment are 407 ± 5 emu/cm^3(3.26 ± 0.04 $\mu_B/(f.u.)$) and 3.31 ± 0.15 $\mu_B/(f.u.)$, respectively, which are close to the bulk value. The spin polarization at the Fermi level is directly measured

13

using SRPES. The value of spin polarization changes from positive to negative to almost zero, indicating that the oxidation degree of the deposited films is gradually enhanced. A spin polarization value close to the theoretical value is observed in the Fe_3O_4 film as thin as 20 nm. The spin polarization has a maximum value of -42±3% for the 40 nm $Fe_3O_4(001)$ film. Furthermore, the film thickness-dependent measurements indicate that the APBs significantly decrease the spin polarization rather than the lattice mismatch. Our results demonstrate the direct observation of spin polarization in epitaxial $Fe_3O_4(001)$/MgO thin films grown by magnetron sputtering, which provides some insight into the development of Fe_3O_4-based spintronic devices.

SUPPLEMENTARY MATERIAL

See the supplementary material for additional information of the fitting process of XPS spectra, magnetic characterization of the samples grown at different flow fates of O_2, the measurements of the SRPES, and the SRPES spectra and the corresponding spin polarization of the samples grown at different flow fates of O_2.

ACKNOWLEDGEMENTS

DATA AVAILABILITY

The data that support the findings of this work are available from the corresponding author upon reasonable request.

References

[1]R. A. de Groot, F. M. Mueller, P. G. van Engen, and K. H. J. Buschow, Phys. Rev. Lett. **50**, 2024 (1983).

[2]Z. Zhang and S. Satpathy, Phys. Rev. B **44**, 13319 (1991).

[3]Yu S. Dedkov, U. Rüdiger, and G. Güntherodt, Phys. Rev. B **65** (2002).

[4]Manuel Bibes, Javier E. Villegas, and Agnès Barthélémy, Adv. Phys. **60**, 5 (2011).

[5]H. C. Wu, O. N. Mryasov, M. Abid, K. Radican, and I. V. Shvets, Sci. Rep. **3**, 1830 (2013).

[6]Shwetha G. Bhat and P. S. Anil Kumar, Mater. Res. Express **3** (2016).

[7]J. M. De Teresa, A. Fernández-Pacheco, L. Morellon, J. Orna, J. A. Pardo, D. Serrate, P. A. Algarabel, and M. R. Ibarra, Microelectron. Eng. **84**, 1660 (2007).

[8]Y. X. Lu, J. S. Claydon, Y. B. Xu, S. M. Thompson, K. Wilson, and G. van der Laan, Phys. Rev. B **70** (2004).

[9]H. Yanagihara, M. Myoka, D. Isaka, T. Niizeki, K. Mibu, and E. Kita, J. Phys. D: Appl. Phys. **46** (2013).

[10]Tatsuo Fujii, Mikio Takano, Rintaro Katano, Yasuhito Isozumi, and Yoshichika Bando, J. Magn. Magn. Mater. **130**, 267 (1994).

[11]D. J. Huang, C. F. Chang, J. Chen, L. H. Tjeng, A. D. Rata, W. P. Wu, S. C. Chung, H. J. Lin, T. Hibma, and C. T. Chen, J. Magn. Magn. Mater. **239**, 261 (2002).

[12]Victor Ukleev, Mikhail Volkov, Alexander Korovin, Thomas Saerbeck, Nikolai Sokolov, and Sergey Suturin, Phys. Rev. Mater. **3** (2019).

[13]D. Wilson and M. A. Langell, Appl. Surf. Sci. **303**, 6 (2014).

[14]Toru Yamashita and Peter Hayes, J. Electron Spectrosc. **152**, 6 (2006).

[15]C. Ruby, B. Humbert, and J. Fusy, Surf. Interface Anal. **29**, 377 (2000).

[16]D. L. A. de Faria, S. Venâncio Silva, and M. T. de Oliveira, J. Raman Spectrosc. **28**, 873 (1997).

[17]S. Brice-Profeta, M. A. Arrio, E. Tronc, N. Menguy, I. Letard, C. Cartier dit Moulin, M. Noguès, C. Chanéac, J. P. Jolivet, and Ph Sainctavit, J. Magn. Magn. Mater. **288**, 354 (2005).

[18]W. Q. Liu, Y. B. Xu, P. K. J. Wong, N. J. Maltby, S. P. Li, X. F. Wang, J. Du, B. You, J. Wu, P. Bencok, and R. Zhang, Appl. Phys. Lett. **104** (2014).
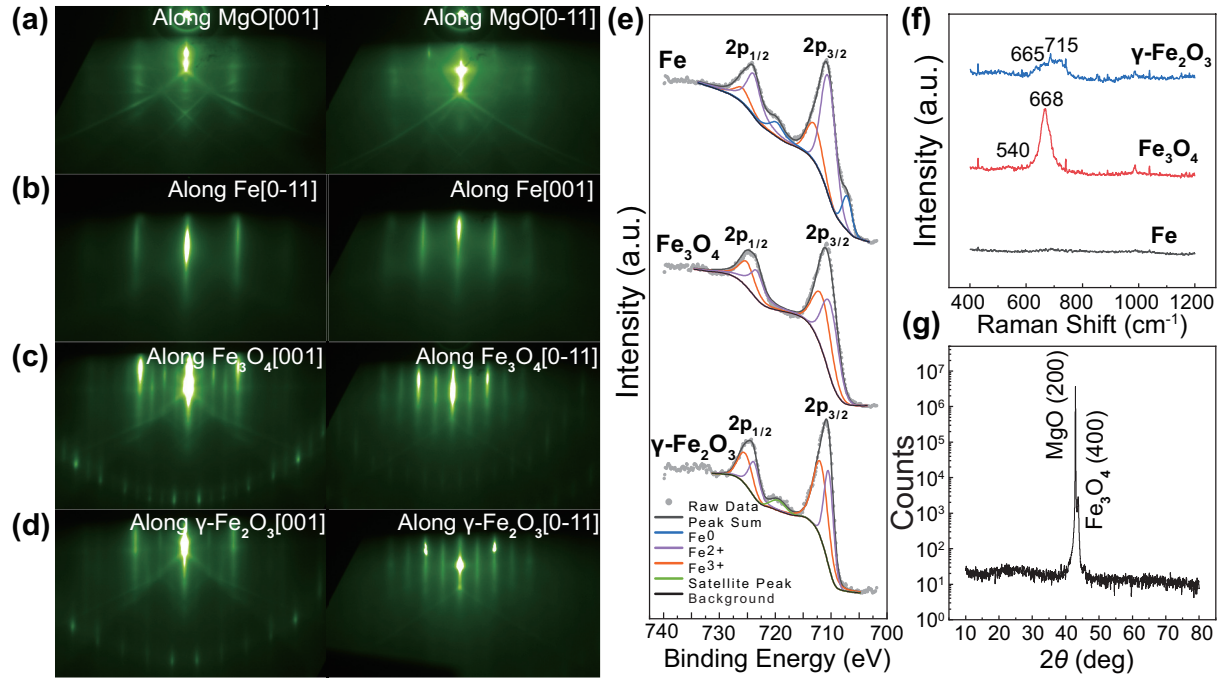
[19] D. J. Huang, C. F. Chang, H. T. Jeng, G. Y. Guo, H. J. Lin, W. B. Wu, H. C. Ku, A. Fujimori, Y. Takahashi, and C. T. Chen, Phys. Rev. Lett. **93**, 077204 (2004).

[20] C. T. Chen, Y. U. Idzerda, H. Lin, N. V. Smith, G. Meigs, E. Chaban, G. H. Ho, E. Pellegrin, and F. Sette, Phys. Rev. Lett. **75**, 152 (1995).

[21] V. Hari Babu, R. K. Govind, K. M. Schindler, M. Welke, and R. Denecke, J. Appl. Phys. **114** (2013).

[22] W. G. Wang, M. Li, S. Hageman, and C. L. Chien, Nat. Mater. **11**, 64 (2011).

[23] Kang L. Wang, Xufeng Kou, Pramey Upadhyaya, Yabin Fan, Qiming Shao, Guoqiang Yu, and Pedram Khalili Amiri, Proc. IEEE **104**, 1974 (2016).

[24] S. A. Wolf, D. D. Awschalom, R. A. Buhrman, J. M. Daughton, S. von Molnar, M. L. Roukes, A. Y. Chtchelkanova, and D. M. Treger, Science **294**, 1488 (2001).

[25] Yu Yan, Xianyang Lu, Bo Liu, Xiaoqian Zhang, Xiangyu Zheng, Hao Meng, Wenqing Liu, Junlin Wang, Iain G. Will, Jing Wu, Ping Kwan Johnny Wong, Jianwang Cai, Jun Du, Rong Zhang, and Yongbing Xu, J. Appl. Phys. **127** (2020).

[26] N. T. H. Kim-Ngan, A. G. Balogh, J. D. Meyer, J. Brötz, S. Hummelt, M. Zając, T. Ślęzak, and J. Korecki, Nucl. Instrum. Methods Phys. Res. B **267**, 1484 (2009).

[27] F. C. Voogt, T. T. M. Palstra, L. Niesen, O. C. Rogojanu, M. A. James, and T. Hibma, Phys. Rev. B **57**, R8107 (1998).

[28] D. T. Margulies, F. T. Parker, M. L. Rudee, F. E. Spada, J. N. Chapman, P. R. Aitchison, and A. E. Berkowitz, Phys. Rev. Lett. **79**, 5162 (1997).

[29] M. Fonin, R. Pentcheva, Yu S. Dedkov, M. Sperlich, D. V. Vyalikh, M. Scheffler, U. Rüdiger, and G. Güntherodt, Phys. Rev. B **72** (2005).

[30] M. Schmitt, O. Kirilmaz, S. Chernov, S. Babenkov, D. Vasilyev, O. Fedchenko, K. Medjanik, Yu Matveyev, A. Gloskovskii, C. Schlueter, A. Winkelmann, L. Dudy, H. J. Elmers, G. Schönhense, M. Sing, and R. Claessen, Phys. Rev. B **104** (2021).

[31] G. Mariotto, S. Murphy, and I. V. Shvets, Phys. Rev. B **66** (2002).

[32] R. Pentcheva, W. Moritz, J. Rundgren, S. Frank, D. Schrupp, and M. Scheffler, Surf. Sci. **602**, 1299 (2008).

[33] W. Wang, J. M. Mariot, M. C. Richter, O. Heckmann, W. Ndiaye, P. De Padova, A. Taleb-Ibrahimi, P. Le Fèvre, F. Bertran, F. Bondino, E. Magnano, J. Krempaský, P. Blaha, C. Cacho, F. Parmigiani, and K. Hricovini, Phys. Rev. B **87** (2013).

[34] S. Monastra, F. Manghi, C. A. Rozzi, C. Arcangeli, E. Wetli, H. J. Neff, T. Greber, and J. Osterwalder, Phys. Rev. Lett. **88**, 236402 (2002).

[35] Hui Liu, E. Y. Jiang, H. L. Bai, R. K. Zheng, and X. X. Zhang, J. Phys. D: Appl. Phys. **36**, 2950 (2003).

[36] W. Eerenstein, T. T. M. Palstra, T. Hibma, and S. Celotto, Phys. Rev. B **68** (2003).

[37] W. Eerenstein, T. T. M. Palstra, and T. Hibma, Thin Solid Films **400**, 90 (2001).

[38] K. P. McKenna, F. Hofer, D. Gilks, V. K. Lazarov, C. Chen, Z. Wang, and Y. Ikuhara, Nat. Commun. **5**, 5740 (2014).
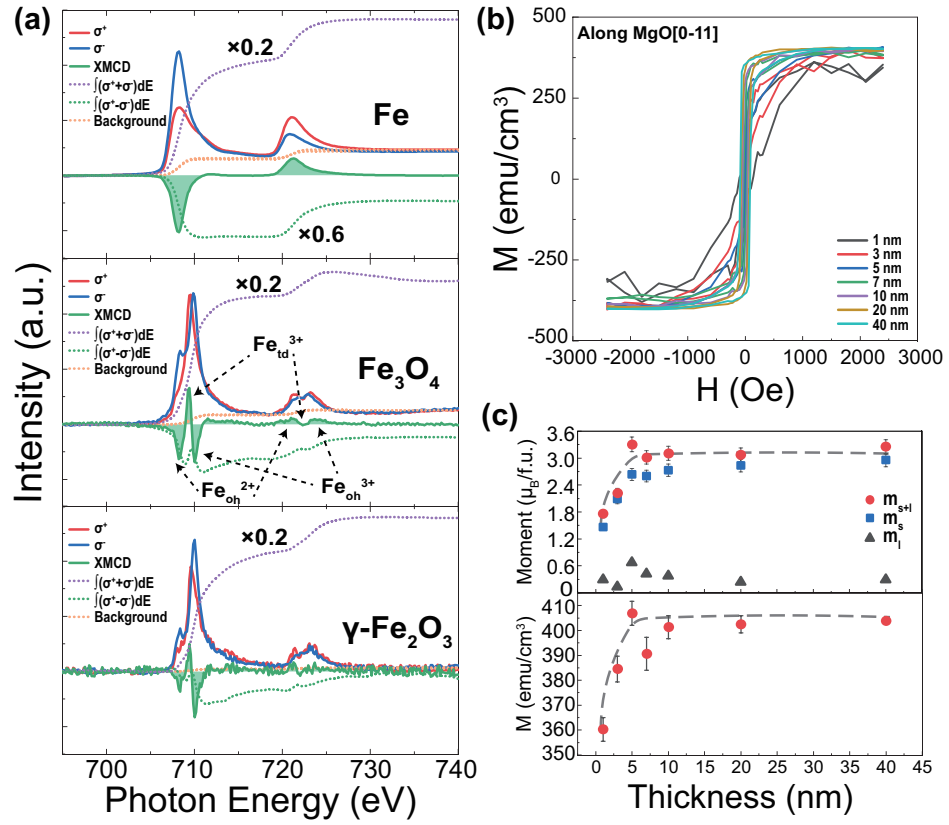
16

(a) Along MgO[001] Along MgO[0-11]
(b) Along Fe[0-11] Along Fe[001]
(c) Along Fe$_3$O$_4$[001] Along Fe$_3$O$_4$[0-11]
(d) Along γ-Fe$_2$O$_3$[001] Along γ-Fe$_2$O$_3$[0-11]

(e) Fe 2p$_{1/2}$ 2p$_{3/2}$
Fe$_3$O$_4$ 2p$_{1/2}$ 2p$_{3/2}$
γ-Fe$_2$O$_3$ 2p$_{1/2}$ 2p$_{3/2}$

Intensity (a.u.)

Raw Data
Peak Sum
Fe0
Fe2+
Fe3+
Satellite Peak
Background

740 730 720 710 700
Binding Energy (eV)

(f) γ-Fe$_2$O$_3$ 665 715
Fe$_3$O$_4$ 668 540
Fe

Intensity (a.u.)

400 600 800 1000 1200
Raman Shift (cm^{-1})

(g)
10^7
10^6
10^5
10^4
10^3
10^2
10^1
10^0

Counts

MgO (200)
Fe$_3$O$_4$ (400)

10 20 30 40 50 60 70 80
2θ (deg)

(a)

σ⁺
σ⁻
XMCD
∫(σ⁺+σ⁻)dE
∫(σ⁺-σ⁻)dE
Background

×0.2

Fe

×0.6

Fe₃O₄

×0.2

Fe$_{td}$³⁺

Fe$_{oh}$²⁺

Fe$_{oh}$³⁺

γ-Fe₂O₃

×0.2

Intensity (a.u.)

Photon Energy (eV)

(b)

Along MgO[0-11]

M (emu/cm³)

H (Oe)

1 nm
3 nm
5 nm
7 nm
10 nm
20 nm
40 nm

(c)

Moment (μ$_B$/f.u.)

m$_{s+l}$
m$_s$
m$_l$

M (emu/cm³)

Thickness (nm)